

Electronic structure of single-crystalline $\text{Mg}_x\text{Al}_{1-x}\text{B}_2$ probed by x-ray diffraction multipole refinements and polarization-dependent x-ray absorption spectroscopy

M. Merz,^{1,2,*} P. Schweiss,¹ Th. Wolf,¹ H. v. Löhneysen,^{1,3} and S. Schuppler¹

¹*Institut für Festkörperphysik, Karlsruhe Institute of Technology, 76021 Karlsruhe, Germany*

²*Institut für Kristallographie, Rheinisch-Westfälische Technische Hochschule Aachen, 52056 Aachen, Germany*

³*Physikalisches Institut, Karlsruhe Institute of Technology, 76131 Karlsruhe, Germany*

(Dated: February 26, 2024)

X-ray diffraction multipole refinements of single-crystalline $\text{Mg}_x\text{Al}_{1-x}\text{B}_2$ and polarization-dependent near-edge x-ray absorption fine structure at the B 1s edge reveal a strongly anisotropic electronic structure. Comparing the data for superconducting compounds ($x = 0.8, 1.0$) with those for the non-superconductor ($x = 0$) gives direct evidence for a rearrangement of the hybridizations of the boron p_z bonds and underline the importance of holes in the σ -bonded covalent sp^2 states for the superconducting properties of the diborides. The data indicate that Mg is approximately divalent in MgB_2 and suggest predominantly ionic bonds between the Mg ions and the two-dimensional B rings. For AlB_2 ($x = 0$), on the other hand, about 1.5 electrons per Al atom are transferred to the B sheets while the residual 1.5 electrons remain at the Al site which suggests significant covalent bonding between the Al ions and the B sheets. This finding together with the static electron deformation density points to almost equivalent electron counts on B sheets of MgB_2 and AlB_2 , yet with a completely different electron/hole distribution between the σ and π bonds.

PACS numbers: 74.70.Ad, 78.70.Dm, 74.25.Jb, 74.62.Dh

I. INTRODUCTION

Since the discovery of superconductivity in MgB_2 with a transition temperature $T_c \approx 39$ K,¹ which is high for a binary compound, this material has been intensely studied, and now many properties of MgB_2 seem to be well understood. Compared to the high- T_c cuprates or the recently discovered iron pnictides, the crystal structure is simple: in its space group $P6/mmm$ magnesium and boron reside on special positions at 0,0,0 and $\frac{1}{3}, \frac{2}{3}, \frac{1}{2}$, respectively, and form separate layers which, for B, are graphite-like with a hexagonal atomic arrangement. The B rings and the intercalated Mg sheets are stacked alternately along the c axis as illustrated in Fig. 1. This layered structure, and especially the covalent sp^2 and two-dimensional character of the B-B σ bonds,² suggests a strong anisotropy between in-plane and out-of-plane properties.³ Indeed, band-structure calculations predict two degenerate two-dimensional σ bands and two three-dimensional π bands around the Fermi level E_F .^{2,4-6} Initially it was inferred from experiment and theory that superconductivity in this compound is conventional, being s -wave, BCS-type, and phonon-induced.⁷⁻¹⁰ Yet quite early on, deviations were observed, like the presence of two energy gaps of about 7 meV and 2.5 meV related to the σ and π bands, respectively.¹¹⁻¹⁴ As a result, the superconducting state of MgB_2 is presently understood within a multiband approach of the Eliashberg theory where the pairing is split into σ and π intraband and σ - π interband contributions.^{11,15-18} It has been demonstrated that the coupling between the σ -band electrons and the B-B bond-stretching phonon mode with E_{2g} symmetry at the Γ point plays a decisive role for superconductivity in MgB_2 .^{9,15,19-21} The electron-phonon coupling for the π bands and the interband coupling seem to be weaker

although not negligible.¹⁷

Much work has concentrated on a direct determination of the spatial, electronic, and vibrational properties and the superconducting gap structure of MgB_2 . A complementary approach is to investigate systems obtained from the superconducting parent compound by substituting characteristic elements, thereby reducing or even suppressing the superconducting state.²² In this respect, the $\text{Mg}_x\text{Al}_{1-x}\text{B}_2$ system poses an interesting example where superconductivity is suppressed upon replacing formally divalent Mg with formally trivalent Al. Preparation of $\text{Mg}_x\text{Al}_{1-x}\text{B}_2$ single crystals where Mg is partially or completely replaced by Al is possible for all concentrations. Across the entire doping range $0 \leq x \leq 1$ the crystal structure is preserved while T_c is considerably reduced with decreasing x and finally disappears around $x \lesssim 0.6$.²³ Up to now, several mechanisms like band filling due to substitution of Mg^{2+} with Al^{3+} , merging of the superconducting gaps, increased interband scattering, and a decrease in the electron-phonon coupling (Refs. 18, 19, 23-27) have been suggested to explain the very rapidly reduced superconductivity at only modest substitution levels.²⁸ So far, however, a consistent picture is elusive and a direct investigation of the electronic structure and the bonding characteristics of the sp^2 and p_z states in $\text{Mg}_x\text{Al}_{1-x}\text{B}_2$ might help in an understanding of the suppression of superconductivity in $\text{Mg}_x\text{Al}_{1-x}\text{B}_2$ for $x \lesssim 0.6$ and of the changes of the electronic structure especially in the less investigated doping range $0 \leq x < 0.6$.

To shed more light on the doping-dependent suppression of the superconducting state and to study the changes in the electronic structure, we have investigated $\text{Mg}_x\text{Al}_{1-x}\text{B}_2$ single crystals employing x-ray diffraction multipole refinements and polarization-dependent near-edge x-ray absorption fine structure (NEXAFS). X-ray

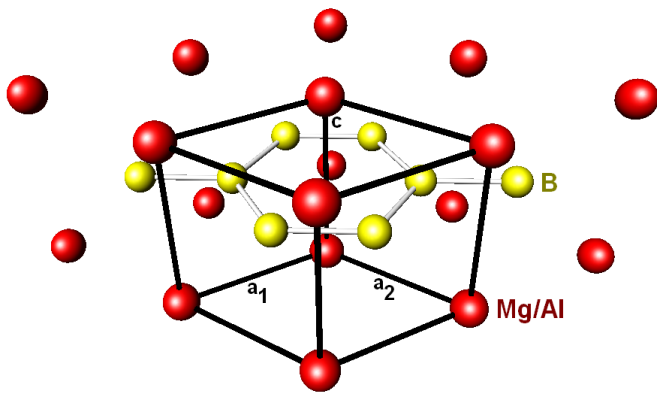


Figure 1. (Color online) Unit cell of $Mg_xAl_{1-x}B_2$. The red and yellow spheres correspond to the (Mg,Al) and B sites. In its space group $P6/mmm$ magnesium/aluminum and boron reside on special positions at $0,0,0$ and $\frac{1}{3}, \frac{2}{3}, \frac{1}{2}$, respectively. The B rings and the intercalated Mg sheets have a hexagonal atomic arrangement and are stacked alternately along the c axis.

diffraction multipole refinements give direct information about the bonding nature of the relevant electronic states, while NEXAFS tracks the doping-dependent changes in the orbital states and/or in the electronic band structure. The current data provide experimental evidence that Mg is approximately divalent in $Mg_xAl_{1-x}B_2$ and suggest a predominantly ionic bonding of the Mg ions and the B layers while Al has a residual valence of ≈ 1.5 electrons and exhibits significant covalent bonding between the Al atoms and the B sheets. This leads for MgB_2 and AlB_2 to almost equivalent electron counts on B sites, yet with a completely different electron/hole distribution between the σ and π bonds. The present data also demonstrate that the doping-dependent filling of σ -bonded covalent sp^2 states goes along with a change of the bonding nature of the π -bonded p_z orbitals.

II. EXPERIMENTAL

AlB_2 and $Mg_{0.8}Al_{0.2}B_2$ single crystals were grown from Al or Al/Mg flux by the slow-cooling method. The resulting crystals have hexagonal (001) surfaces with sizes of about $2 \times 2 \text{ mm}^2$ for $x = 0$ and $0.4 \times 0.5 \text{ mm}^2$ for $x = 0.8$. Hexagonal single-crystalline MgB_2 platelets with a diameter of up to $200 \mu\text{m}$ are obtained by isothermally annealing ^{11}B powder in a Mg flux enclosed in an evacuated Mo cylinder.²⁹ The MgB_2 crystals show a sharp superconducting transition at $T_c = 38.8 \text{ K}$, with a resistive 10 - 90% width $\Delta T \approx 1.8 \text{ K}$. For $Mg_{0.8}Al_{0.2}B_2$ the transition is already reduced to around 20 K and considerably broadened and for AlB_2 superconductivity is completely absent.

X-ray diffraction data were collected at room temperature on a Stoe four-circle diffractometer (equipped with a pyrolytic graphite monochromator) using Mo $K\alpha_{1,2}$ ra-

diation. All accessible symmetry-equivalent reflections of MgB_2 , $Mg_{0.8}Al_{0.2}B_2$, and AlB_2 were measured up to a maximum angle 2θ of 127.5° ($\sin \Theta/\lambda = 1.26 \text{ \AA}^{-1}$). The data were corrected for Lorentz, polarization, extinction, and absorption effects. 92 and 103 averaged symmetry-independent reflections ($I > 3\sigma$) have been included for the multipole treatment of MgB_2 and AlB_2 , respectively. The electron density was refined using the Hansen-Coppens formalism^{30,31}

$$\rho_{atom}(\mathbf{r}) = \rho_{core}(r) + P_\nu \cdot \kappa_1^3 \cdot \rho_{\text{spher, valence}}(\kappa_1 r) \quad (1) \\ + \sum_{l=1}^4 \kappa_2^3 \cdot R_l(\kappa_2 r) \cdot \sum_{m=-l}^l P_{lm\pm} y_{lm\pm}(\mathbf{r}/r)$$

where $\rho_{core}(r)$ is the contribution from the core electrons; the second and third term describe the spherical and multipolar contribution of the valence-electron density, respectively; κ_1 and κ_2 are contraction/expansion parameters of the valence shell, R_l Slater-type radial functions, and $y_{lm\pm}$ spherical harmonics. The electron populations P_ν and $P_{lm\pm}$ are determined during the least-squares refinement. According to the $\bar{6}m2$ symmetry of the B position, P_ν , P_{20} , and P_{33-} values were refined; for the (Mg,Al) site with $6/mmm$ symmetry P_ν and P_{20} were determined to correctly describe the valence-electron distribution at this site.

During the refinement, the high-order reflections with a cutoff of $\sin \Theta/\lambda = 0.9 \text{ \AA}^{-1}$ were used to obtain in a

Table I. Structural parameters of $Mg_xAl_{1-x}B_2$ for $x = 1.0$, $x = 0.8$, and $x = 0.0$. The position of Mg/Al is at $0,0,0$ and that of B at $\frac{1}{3}, \frac{2}{3}, \frac{1}{2}$; $\alpha = 90^\circ$, $\gamma = 120^\circ$. The U_{ii} denote the atomic displacement factors ($U_{22} = U_{11}$; $U_{12} = 0.5 \cdot U_{11}$). The site occupancy factor SOF of B is fixed to 1.

		$x = 1.0$	$x = 0.8$	$x = 0.0$
	wR_2 (%)	1.85	4.44	0.97
	a (\AA)	3.085(1)	3.071(1)	3.003(1)
	c (\AA)	3.522(1)	3.484(1)	3.254(1)
Mg/Al	U_{11} (\AA^2)	0.0051(2)	0.0048(1)	0.0077(1)
	U_{33} (\AA^2)	0.0057(3)	0.0060(1)	0.0061(1)
	SOF	1.0	0.99	0.93
	κ_1	0.89(41)		1.51(8)
	κ_2	1.62(41)		1.30(5)
	P_ν	0.38(21)		1.46(10)
	P_{20}	0.09(3)		0.43(4)
B	U_{11} (\AA^2)	0.0039(2)	0.0039(1)	0.0039(1)
	U_{33} (\AA^2)	0.0061(3)	0.0068(2)	0.0062(1)
	κ_1	0.87(2)		1.01(2)
	κ_2	0.91(8)		0.85(4)
	P_ν	3.82(10)		3.73(4)
	P_{20}	-0.07(3)		0.18(1)
	P_{33-}	-0.24(4)		-0.21(3)
Mg/Al-B distance	d_1 (\AA)	2.505(2)	2.486(2)	2.378(2)
B-B distance	d_2 (\AA)	1.781(1)	1.773(1)	1.734(1)

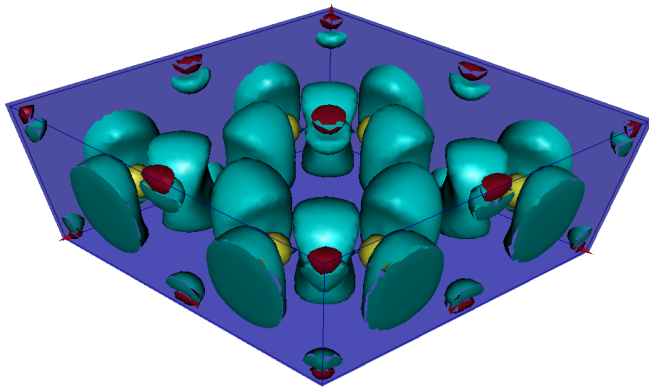


Figure 2. (Color online) Static deformation electron density of MgB_2 (turquoise) shown for an isosurface of $0.02 e/\text{\AA}^3$. The red and yellow spheres correspond to the Mg and B sites, respectively (see also unit cell in Fig. 1). The electrons predominantly reside on σ -bonded sp^2 hybrids and π -bonded p_z orbitals, i. e., between the B sites. The small electron count found at the Mg site might point to a weak hybridization between Mg $3s/3p$ and B p_z states.

first step a good estimate for preliminary anisotropic displacement parameters (ADP's). It should be noted that the atomic positions do not have to be refined since all (Mg,Al) and B atoms reside at special positions in the unit cell. In a second step, the ADP's were fixed and the multipolar refinement of the electron-density parameters was performed using all reflections. Finally, the ADP's were relaxed as well and refined together with all multipolar parameters. The refinements converged very well and the weighted reliability factors (wR_2) strongly decreased from about 4% for a conventional refinement to ≈ 1 -2% for the multipolar treatment. For the multipolar refinements of MgB_2 and AlB_2 , only a marginal residual electron density is found in the difference Fourier synthesis, which together with the good wR_2 values underlines the excellent agreement between the multipole model and the measured data. The multipole parameters obtained in this way were used to calculate the static deformation electron density which characterizes the redistribution of electrons in relation to a crystal built from spherical atoms³² and, thus, describes the bonding characteristics of the valence electrons. Due to the increased disorder expected for the (Mg,Al) position, no multipole modeling was tried for $\text{Mg}_{0.8}\text{Al}_{0.2}\text{B}_2$.

Using linearly polarized light, NEXAFS measurements at the B $1s$ edge were performed for AlB_2 at beamline U4B at the National Synchrotron Light Source (NSLS), Upton, NY, USA, and for $\text{Mg}_{0.8}\text{Al}_{0.2}\text{B}_2$ and MgB_2 at beamline U5 at the National Synchrotron Radiation Research Center (NSRRC), Hsinchu, Taiwan. Resolution was set to 180 and 100 meV at the NSLS and the NSRRC, respectively. All data were taken at room temperature employing bulk-sensitive fluorescence yield (FY), and were corrected for self-absorption effects using the method outlined in Ref. 22. Applying dipole

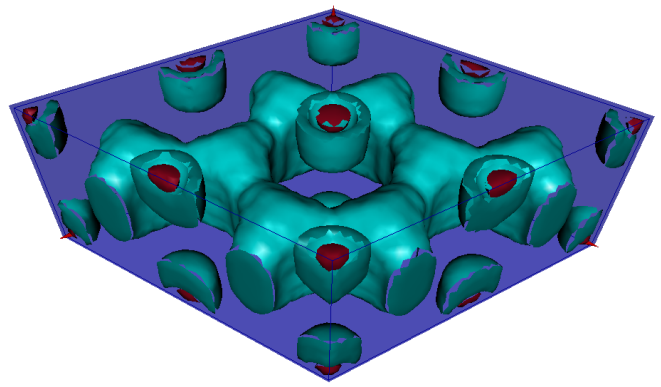


Figure 3. (Color online) Static deformation electron density of AlB_2 (turquoise) shown for an isosurface of $0.02 e/\text{\AA}^3$. The red spheres correspond to the Al sites (see also unit cell in Fig. 1); the B ions are located below the bulge of the isosurface ring. The σ -bonded sp^2 hybrids are entirely filled with electrons whereas the bulge above and below the B sites together with the electrons found on Al ions point to a hybridization between Al $3s/3p$ and B p_z states.

selection rules, the unoccupied part of the B $2p$ final states can be reached from the initial B $1s$ core level. Thus, polarization-dependent NEXAFS measurements on hexagonal $\text{Mg}_{1-x}\text{Al}_x\text{B}_2$ single crystals provide insight into the symmetry of the hole states at E_F with B $2p$ character. While the in-plane $\mathbf{E} \perp \mathbf{c}$ spectrum is obtained for a normal-incidence alignment, i. e., for a grazing angle θ of 0° , the out-of-plane $\mathbf{E} \parallel \mathbf{c}$ spectrum is determined by measuring in a grazing-incidence setup with a grazing angle of 60° and by extrapolating the spectra to $\theta = 90^\circ$.

III. RESULTS AND DISCUSSION

The results of the x-ray diffraction refinements are summarized in Table I. The lattice parameters and the ADP's of our single crystals are consistent with established values.³³⁻³⁶ It is evident that the a and c lattice parameters strongly shrink when going from MgB_2 to $\text{Mg}_{0.8}\text{Al}_{0.2}\text{B}_2$ and AlB_2 . Moreover, our multipole refinement of MgB_2 is in agreement with published results.³² In contrast to Ref. 32, the Mg site is completely occupied in our MgB_2 samples. For the AlB_2 sample, on the other hand, the previously observed slightly reduced 93 % occupation of the Al position³⁷ also shows up in our investigations. According to the present MgB_2 refinement, the valence electron count of Mg is $\approx 0.4(2)$ and that of B $\approx 3.8(1)$, indicating that the two valence electrons of Mg are mostly but not entirely transferred to the B layer. To visualize the valence electron distribution, the static deformation electron density of MgB_2 is depicted in Fig. 2. It has the shape of a molar and unambiguously resides between the B sites on σ -bonded sp^2 hybrids and (banana-shaped) π -bonded p_z orbitals. Yet both hybrid states seem to be not *completely* filled (no deformation electron

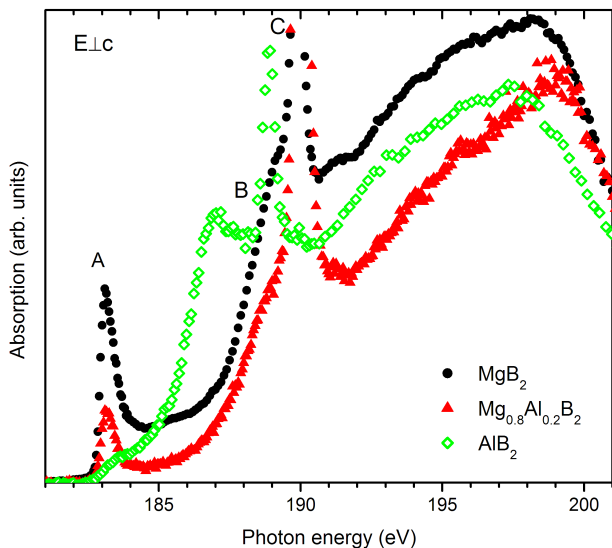


Figure 4. (Color online) Orbital-specific electronic structure of single-crystalline MgB_2 , $\text{Mg}_{0.8}\text{Al}_{0.2}\text{B}_2$, and AlB_2 : B $1s$ NEXAFS with $\mathbf{E}\perp\mathbf{c}$, probing unoccupied σ -bonded B $2p_{xy}$ and π -bonded B $2p_z$ states.

density is found around the B sites). Two-dimensional cuts through our three-dimensional plot of the static deformation electron density are absolutely consistent with the deformation density maps given in Ref. 32. In agreement with Ref. 32, a small residual number of electrons is found above and below the Mg site (see Fig. 2 and Table I). Such a small electron count at the Mg site might point to a weak hybridization between the Mg ion and the B p_z orbitals.

The situation is, however, quite different for AlB_2 . The multiple refinement of AlB_2 summarized in Table I clearly shows that not all three but only $\approx 1.5(1)$ valence electrons are transferred from the Al site to the B layer while an equal amount of $1.5(1)$ electrons remains at the Al site. As a consequence this leads to almost equivalent electron counts of ≈ 3.8 for the B layers in MgB_2 and of ≈ 3.7 for those in AlB_2 , albeit with a significantly different electron/hole distribution between the σ and π bonds. In order to show this, let us compare the static deformation electron density of AlB_2 in Fig. 3 with that of MgB_2 described above and shown in Fig. 1. For AlB_2 the isosurface has the shape of a ring, thereby essentially resembling the hexagonal arrangement of the B ions. Moreover, the comparison of the static deformation electron density of MgB_2 and AlB_2 suggests that in the case of AlB_2 the σ -bonded sp^2 states are completely filled with electrons and shows that the maximum in the electron density of the p_z orbitals does no longer appear *between* the B sites but rather *at* these sites, thereby leading for the isosurface to a bulge above and below the B sites. In addition, a certain electron count is clearly visible around the Al site. Compared to MgB_2 , the electron density at the (Mg,Al) site is strongly enhanced for AlB_2 and, in contrast to MgB_2 , the electron density does

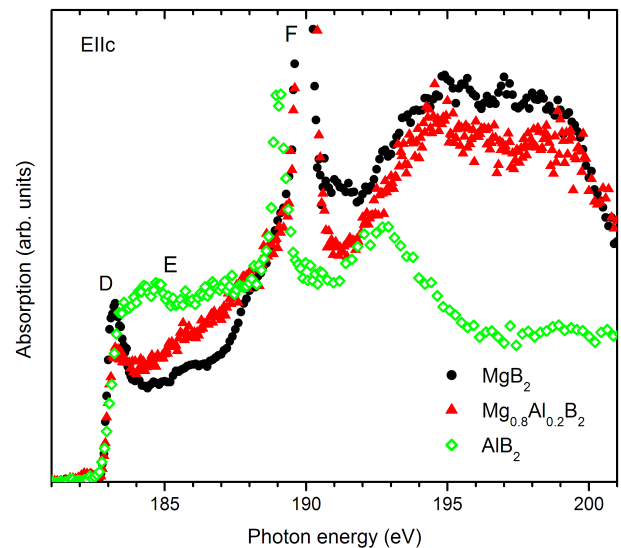


Figure 5. (Color online) Orbital-specific electronic structure of single-crystalline MgB_2 , $\text{Mg}_{0.8}\text{Al}_{0.2}\text{B}_2$, and AlB_2 : B $1s$ NEXAFS with $\mathbf{E}\parallel\mathbf{c}$, probing unoccupied π -bonded B $2p_z$ states.

not only reside above and below the (Mg,Al) site but rather completely surrounds the Al ion. This finding, together with the 1.5 electrons found on Al sites (see Fig. 3 and Table I) and the bulge above and below the B sites, points to strong hybridization between Al $3s/3p$ and B p_z states as suggested in Ref. 38. Simultaneously, a non-negligible amount of in-plane holes seems to persist on the π -bonded p_z orbitals. (Compared to MgB_2 a strongly reduced electron density is found between the B sites on banana-shaped π -bonded p_z orbitals.) Therefore, two effects occur with increasing Al content: Firstly, the σ -bonded sp^2 states become filled with electrons and, secondly, the p_z orbitals begin to hybridize strongly with those at the (Mg,Al) site. This second effect changes the bonding nature between the (Mg,Al) site and the B sheets from predominantly ionic for MgB_2 to covalent for AlB_2 . These changes are fully consistent with first-principles studies using the virtual crystal approximation where a charge transfer from the B-B σ bonds to the π bonds in the inter-planar region was observed.^{23,38} Our data also agree with the detailed supercell calculations in Ref. 38 where it was shown that covalent bond clusters composed of Al and the adjacent four B-B bonds emerge upon Al substitution. As a consequence of this increasingly covalent character of the bonds, the (Mg/Al)-B bond length is reduced as well, from 2.505 to 2.486 and 2.378 Å when decreasing the Mg content from $x = 1.0$ to 0.8 and finally 0 (see Table I).

Further support for the successive filling of the σ bands and the simultaneous change in the bonding nature of the π states comes from the in-plane ($\mathbf{E}\perp\mathbf{c}$) and out-of-plane ($\mathbf{E}\parallel\mathbf{c}$) boron K edge NEXAFS spectra of MgB_2 , $\text{Mg}_{0.8}\text{Al}_{0.2}\text{B}_2$, and AlB_2 displayed between 180 and 201 eV in Figs. 4 and 5, respectively. In this energy range

the spectra reflect the unoccupied boron $2p$ density of states at E_F and several eV above. For the $\mathbf{E}\perp\mathbf{c}$ spectrum in Fig. 4, a sharp peak (feature A) appears around E_F for MgB_2 . When going from MgB_2 to $\text{Mg}_{0.8}\text{Al}_{0.2}\text{B}_2$ and AlB_2 , a substantial decrease of feature A is immediately obvious. This reduction of feature A which has already been reported in literature^{25,39–43} illustrates that the σ -bonded boron sp^2 states become gradually occupied upon Al doping and are finally located below E_F for AlB_2 . Consistent with the shift of the maximum position towards the boron sites observed for the static deformation density of AlB_2 in Fig. 3, the residual states found in Fig. 4 for feature A may be attributed to a small amount of in-plane holes residing on π -bonded boron $2p_z$ orbitals, i. e., between the boron sites. Following Ref. 42, structures B and C of Fig. 4 are ascribed to antibonding σ^* states and the so-called resonance peak, respectively. The latter is either related to oxide impurities or has its origin in resonant elastic scattering³⁹ and will not be discussed here. In any case, the antibonding σ^* states (feature B) located for MgB_2 about 6 eV above E_F (for $x = 0.8$ and 1.0 they only appear as a preceding shoulder of the resonance peak) are shifted by 1 eV towards E_F , but clearly remain unoccupied when going from MgB_2 to AlB_2 .

In the out-of-plane ($\mathbf{E}\parallel\mathbf{c}$) spectra in Fig. 5, a sharp peak (feature D) is observed right at E_F for MgB_2 which can be attributed to π -bonded p_z orbitals in the B rings. When going from MgB_2 to $\text{Mg}_{0.8}\text{Al}_{0.2}\text{B}_2$ and AlB_2 , the spectral weight of feature D is significantly reduced while feature E continuously evolves upon increasing Al content, thereby leading for AlB_2 to an increased but almost constant density of states in the energy range between E_F and several eV above. Such a constant density of states may point to hybridizations of wide bands. Taking the shown above multipole refinements into account this finding reflects the strong hybridization between Al $3s/3p$ and B p_z states. Interestingly, feature E already shows up for MgB_2 , yet with significantly reduced spectral weight compared to AlB_2 . As discussed above in the context of the static deformation electron density of MgB_2 , this might point to very weak hybridization between the Mg ion and the B sheets. Similarly to the in-plane spectra, feature F around 190 eV can be ascribed to the resonance peak.

Given that $\text{Mg}_x\text{Al}_{1-x}\text{B}_2$ is a two-band superconductor for which the two-gap characteristic is preserved over almost the entire superconducting range,^{26,44–47} not only the filling of the σ -bonded sp^2 states but also the changes in hybridization between the (Mg,Al) $3s/3p$ and B p_z orbitals observed in our experiments might play an important role for the rapid doping-dependent reduction of T_c . It was shown (e. g., in Refs. 17, 24, and 48) that superconductivity on the σ bands of $\text{Mg}_x\text{Al}_{1-x}\text{B}_2$ is dominated by σ -intraband pairing, whereas π -intraband pairing and σ - π interband coupling are the prominent ingredients for superconductivity on the π bands. Therefore, our data underline that a significant lowering of T_c upon

Al doping can be attributed to σ -band hole filling (and, thus, to reduced σ -intraband pairing). Simultaneously with the σ -band filling, the σ - π interband coupling is strongly altered while, at least to first approximation, the π -intraband pairing is expected to remain unaffected by σ -band filling. However, the electronic structure together with the π -intraband pairing will be completely modified by the changes in the hybridization between the (Mg,Al) $3s/3p$ and B p_z orbitals observed in our diffraction and NEXAFS results. It might, therefore, be expected that the doping-dependent changes observed in the bonding nature between the (Mg,Al) and the B sites are also an important contribution to the particularly rapid decrease of T_c upon Al doping. The modified electronic structure resulting from the changed bonding nature might also explain the absence of the hole-like π sheet for Al-doped samples in de Haas-van Alphen investigations.⁴⁹ Moreover, such changes in the bonding nature are not expected for the replacement of B with C since the local point symmetry in the π and σ orbitals is only affected in the case of Mg substitution by Al.⁵⁰ Indeed the strong reduction of the lattice parameters and of the (Mg,Al)-B bond distance observed for Mg substitution by Al (see Table I) is completely absent for B replacement with C.⁵¹ Consequently, photoemission studies on $\text{Mg}(\text{B}_{1-x}\text{C}_x)_2$ indicate that the σ gap is proportional to T_c while the π gap shows negligible change with increasing B content.⁵² This finding for $\text{Mg}(\text{B}_{1-x}\text{C}_x)_2$ is in contrast to the $\text{Mg}_x\text{Al}_{1-x}\text{B}_2$ system where, according to our data, it is expected that the π gap is correlated with the changes in the covalent bonding nature between (Mg/Al) and B.

IV. SUMMARY AND CONCLUSIONS

To elucidate the doping-dependent suppression of superconductivity in $\text{Mg}_x\text{Al}_{1-x}\text{B}_2$, we have performed multipole refinements of x-ray diffraction data and polarization-dependent near-edge x-ray absorption fine structure on single-crystalline specimens with $x = 1.0, 0.8, \text{ and } 0$. Joined together, our results draw the following picture for the electronic structure and the suppression of superconductivity in $\text{Mg}_x\text{Al}_{1-x}\text{B}_2$: By and large, the Mg ions in MgB_2 are approximately divalent. Despite the residual $\approx 0.4(2)$ electrons remaining at the Mg site, the valence electrons do predominantly reside in the B layers. Neither the σ -bonded B sp^2 nor the π -bonded B p_z orbitals are entirely filled with electrons. This explains the distinctly two-dimensional and covalent character between the B sites with its metallic hole-type conductivity, as well as the appearance of two superconducting energy gaps related to the corresponding σ and π bands. No indication is found for a three-dimensional, delocalized valence-electron density originating from B p_z bonds; neither the multipole model nor the NEXAFS spectra point to a significant electron density outside the B layer – even more so as the distance of about 3.52 Å between neighboring B layers is quite large which effectively reduces

p_z orbital overlap. If anything, the states responsible for three-dimensional metallicity in MgB_2 most probably result from hybridization between $\text{Mg } 3s/3p$ and $\text{B } p_z$ states. Such hybrids also provide a rationale for the electron density remaining at the Mg site.

Upon increasing Al content, the σ -bonded $\text{B } sp^2$ states become successively filled. Yet due to the residual valence electron count of ≈ 1.5 at the Al site as observed in the multipole refinement, the number of electrons in the B layers is only slightly changed from ≈ 3.8 for MgB_2 to ≈ 3.7 for AlB_2 . This finding implies that the σ -bonded $\text{B } sp^2$ states are filled upon replacing Mg by Al at the expense of an increasing hole count of the π -bonded $\text{B } p_z$ states as reflected in the static deformation electron density. Concurrently, the hybridization between $(\text{Mg,Al}) 3s/3p$ orbitals and $\text{B } p_z$ states proceeds with increasing Al content which strongly enhances the covalent bonding nature between (Mg,Al) and B sites. In contrast to MgB_2 where conductivity is dominated by the in-plane σ -bonded $\text{B } sp^2$ states, in AlB_2 the more three-dimensional covalent $\text{Al } 3s/3p$ - $\text{B } p_z$ bond determines the electronic properties.

From the present study it is evident that the filling of the σ -bonded $\text{B } sp^2$ states has a strong impact on the rapidly reduced superconducting transition temperature in $\text{Mg}_x\text{Al}_{1-x}\text{B}_2$. Moreover, it might be expected that the observed changes in the bonding nature between the (Mg,Al) site and the $\text{B } p_z$ orbitals lead to a partic-

ularly rapid decrease of the transition temperature by means of reduced π -intra-band pairing and σ - π interband scattering. Further detailed experimental and theoretical investigations, however, will be needed to show if the observed changes in the hybridization between $(\text{Mg,Al}) 3s/3p$ orbitals and $\text{B } p_z$ states (and the modified electronic structure of the π states caused by these changes) have a decisive role on the superconducting properties of $\text{Mg}_x\text{Al}_{1-x}\text{B}_2$.

ACKNOWLEDGMENTS

We are indebted to G. Roth, G. Heger, and V. Kaiser for fruitful discussions about the multipole refinements. We greatly appreciate generous and excellent experimental help by and helpful discussions with E. Pellegrin, C. T. Chen, S.-C. Chung, S. L. Hulbert, H.-J. Lin, G. Nintzel, S. Tokumitsu, T. Mizokawa, D. A. Arena, J. Dvorak, Y. U. Idzerda, D.-J. Huang, and C.-F. Chang. For stimulating discussions we are grateful to R. Heid, K.-P. Bohnen, and H. Winter. Research was carried out in part at the NSLS, Brookhaven National Laboratory, which is supported by the U. S. Department of Energy, Division of Material Sciences and Division of Chemical Sciences, under contract number DE-AC02-98CH10886.

* Corresponding author: michael.merz@kit.edu

- ¹ J. Nagamatsu, N. Nakagawa, T. Muranaka, Y. Zenitani, and J. Akimitsu, *Nature* **410**, 63 (2001).
- ² J. M. An and W. E. Pickett, *Phys. Rev. Lett.* **86**, 4366 (2001).
- ³ V. Guritanu, A. B. Kuzmenko, D. van der Marel, S. M. Kazakov, N. D. Zhigadlo, and J. Karpinski, *Phys. Rev. B* **73**, 104509 (2006).
- ⁴ J. Kortus, I. I. Mazin, K. D. Belashchenko, V. P. Antropov, and L. L. Boyer, *Phys. Rev. Lett.* **86**, 4656 (2001).
- ⁵ K. D. Belashchenko, M. v. Schilfgaarde, and V. P. Antropov, *Phys. Rev. B* **64**, 092503 (2001).
- ⁶ S. Suzuki, S. Higai, and K. Nakao, *Journal of the Physical Society of Japan* **70**, 1206 (2001).
- ⁷ S. L. Bud'ko, G. Lapertot, C. Petrovic, C. E. Cunningham, N. Anderson, and P. C. Canfield, *Phys. Rev. Lett.* **86**, 1877 (2001).
- ⁸ G. Rubio-Bollinger, H. Suderow, and S. Vieira, *Phys. Rev. Lett.* **86**, 5582 (2001).
- ⁹ K.-P. Bohnen, R. Heid, and B. Renker, *Phys. Rev. Lett.* **86**, 5771 (2001).
- ¹⁰ B. Renker, K.-P. Bohnen, R. Heid, D. Ernst, H. Schober, M. Koza, P. Adelman, P. Schweiss, and T. Wolf, *Phys. Rev. Lett.* **88**, 067001 (2002).
- ¹¹ A. Y. Liu, I. I. Mazin, and J. Kortus, *Phys. Rev. Lett.* **87**, 087005 (2001).
- ¹² X. K. Chen, M. J. Konstantinović, J. C. Irwin, D. D. Lawrie, and J. P. Franck, *Phys. Rev. Lett.* **87**, 157002 (2001).

- ¹³ P. Szabó, P. Samuely, J. Kačmarčík, T. Klein, J. Marcus, D. Fruchart, S. Miraglia, C. Marcanat, and A. G. M. Jansen, *Phys. Rev. Lett.* **87**, 137005 (2001).
- ¹⁴ F. Laube, G. Goll, J. Hagel, H. v. Löhneysen, D. Ernst, and T. Wolf, *EPL (Europhysics Letters)* **56**, 296 (2001).
- ¹⁵ Y. Kong, O. V. Dolgov, O. Jepsen, and O. K. Andersen, *Phys. Rev. B* **64**, 020501 (2001).
- ¹⁶ A. A. Golubov, J. Kortus, O. V. Dolgov, O. Jepsen, Y. Kong, O. K. Andersen, B. J. Gibson, K. Ahn, and R. K. Kremer, *Journal of Physics: Condensed Matter* **14**, 1353 (2002).
- ¹⁷ J. Geerk, R. Schneider, G. Linker, A. G. Zaitsev, R. Heid, K.-P. Bohnen, and H. v. Löhneysen, *Phys. Rev. Lett.* **94**, 227005 (2005).
- ¹⁸ O. De la Peña Seaman, R. de Coss, R. Heid, and K.-P. Bohnen, *Phys. Rev. B* **82**, 224508 (2010).
- ¹⁹ O. De la Peña Seaman, R. de Coss, R. Heid, and K.-P. Bohnen, *Phys. Rev. B* **79**, 134523 (2009).
- ²⁰ A. Q. Baron, H. Uchiyama, S. Tsutsui, Y. Tanaka, D. Ishikawa, J. P. Sutter, S. Lee, S. Tajima, R. Heid, and K.-P. Bohnen, *Physica C: Superconductivity* **456**, 83 (2007).
- ²¹ J. Kortus, *Physica C: Superconductivity* **456**, 54 (2007).
- ²² M. Merz, N. Nücker, E. Pellegrin, P. Schweiss, S. Schuppler, M. Kielwein, M. Knupfer, M. S. Golden, J. Fink, C. T. Chen, et al., *Phys. Rev. B* **55**, 9160 (1997).
- ²³ O. de la Peña, A. Aguayo, and R. de Coss, *Phys. Rev. B* **66**, 012511 (2002).
- ²⁴ J. Kortus, O. V. Dolgov, R. K. Kremer, and A. A. Golubov,

- Phys. Rev. Lett. **94**, 027002 (2005).
- ²⁵ H. D. Yang, H. L. Liu, J.-Y. Lin, M. X. Kuo, P. L. Ho, J. M. Chen, C. U. Jung, M.-S. Park, and S.-I. Lee, Phys. Rev. B **68**, 092505 (2003).
 - ²⁶ R. S. Gonnelli, D. Daghero, A. Calzolari, G. A. Ummarino, V. Dellarocca, V. A. Stepanov, S. M. Kazakov, N. Zhigadlo, and J. Karpinski, Phys. Rev. B **71**, 060503 (2005).
 - ²⁷ T. Masui, S. Lee, and S. Tajima, Phys. Rev. B **70**, 024504 (2004).
 - ²⁸ J. S. Slusky, N. Rogado, K. A. Regan, M. A. Hayward, P. Khalifah, T. He, K. Inumaru, S. M. Loureiro, M. K. Haas, H. W. Zandbergen, et al., Nature **410**, 343 (2001).
 - ²⁹ Pure ^{11}B was used to facilitate neutron scattering on the same samples. (2010).
 - ³⁰ V. Petricek, M. Dusek, and L. Palatinus, Jana2000, (2000). The crystallographic computing system. Institute of Physics, Praha, Czech Republic. (2010).
 - ³¹ N. K. Hansen and P. Coppens, Acta Crystallographica Section A **34**, 909 (1978).
 - ³² V. Tsirelson, A. Stash, M. Kohout, H. Rosner, H. Mori, S. Sato, S. Lee, A. Yamamoto, S. Tajima, and Y. Grin, Acta Crystallographica Section B **59**, 575 (2003).
 - ³³ V. Russell, R. Hirst, F. A. Kanda, and A. J. King, Acta Crystallographica **6**, 870 (1953).
 - ³⁴ M. E. Jones and R. E. Marsh, Journal of the American Chemical Society **76**, 1434 (1954).
 - ³⁵ E. Nishibori, M. Takata, M. Sakata, H. Tanaka, T. Muranaka, and J. Akimitsu, Journal of the Physical Society of Japan **70**, 2252 (2001).
 - ³⁶ H. Mori, S. Lee, A. Yamamoto, S. Tajima, and S. Sato, Phys. Rev. B **65**, 092507 (2002).
 - ³⁷ U. Burkhardt, V. Gurin, F. Haarmann, H. Borrmann, W. Schnelle, A. Yaresko, and Y. Grin, Journal of Solid State Chemistry **177**, 389 (2004).
 - ³⁸ L. Juan, Z. Yuan, and Y. Lin, Communications in Theoretical Physics **49**, 504 (2008).
 - ³⁹ T. A. Callcott, L. Lin, G. T. Woods, G. P. Zhang, J. R. Thompson, M. Paranthaman, and D. L. Ederer, Phys. Rev. B **64**, 132504 (2001).
 - ⁴⁰ J. Nakamura, N. Yamada, K. Kuroki, T. A. Callcott, D. L. Ederer, J. D. Denlinger, and R. C. C. Perera, Phys. Rev. B **64**, 174504 (2001).
 - ⁴¹ J. Nakamura, S.-y. Nasubida, E. Kabasawa, H. Yamazaki, N. Yamada, K. Kuroki, M. Watanabe, T. Oguchi, S. Lee, A. Yamamoto, et al., Phys. Rev. B **68**, 064515 (2003).
 - ⁴² R. F. Klie, J. C. Zheng, Y. Zhu, A. J. Zambano, and L. D. Cooley, Phys. Rev. B **73**, 014513 (2006).
 - ⁴³ A. Mattila, J. A. Soininen, S. Galambosi, T. Pylkkänen, S. Huotari, N. D. Zhigadlo, J. Karpinski, and K. Hämäläinen, Phys. Rev. B **78**, 064517 (2008).
 - ⁴⁴ D. Daghero, D. Delaude, A. Calzolari, M. Tortello, G. A. Ummarino, R. S. Gonnelli, V. A. Stepanov, N. D. Zhigadlo, S. Katrych, and J. Karpinski, Journal of Physics: Condensed Matter **20**, 085225 (2008).
 - ⁴⁵ T. Klein, L. Lyard, J. Marcus, C. Marcenat, P. Szabó, S. Hol'ánová, P. Samuely, B. W. Kang, H.-J. Kim, H.-S. Lee, et al., Phys. Rev. B **73**, 224528 (2006).
 - ⁴⁶ P. Szabó, P. Samuely, Z. Pribulová, M. Angst, S. Bud'ko, P. C. Canfield, and J. Marcus, Phys. Rev. B **75**, 144507 (2007).
 - ⁴⁷ R. Gonnelli, D. Daghero, G. Ummarino, M. Tortello, D. Delaude, V. Stepanov, and J. Karpinski, Physica C: Superconductivity **456**, 134 (2007), ISSN 0921-4534, recent Advances in MgB2 Research.
 - ⁴⁸ T. Dahm and N. Schopohl, Phys. Rev. Lett. **91**, 017001 (2003).
 - ⁴⁹ A. Carrington, J. D. Fletcher, J. R. Cooper, O. J. Taylor, L. Balicas, N. D. Zhigadlo, S. M. Kazakov, J. Karpinski, J. P. H. Charmant, and J. Kortus, Phys. Rev. B **72**, 060507 (2005).
 - ⁵⁰ S. C. Erwin and I. I. Mazin, Phys. Rev. B **68**, 132505 (2003).
 - ⁵¹ M. Paranthaman, J. Thompson, and D. Christen, Physica C: Superconductivity **355**, 1 (2001), ISSN 0921-4534.
 - ⁵² S. Tsuda, T. Yokoya, T. Kiss, T. Shimojima, S. Shin, T. Togashi, S. Watanabe, C. Zhang, C. T. Chen, S. Lee, et al., Phys. Rev. B **72**, 064527 (2005).